2014 IEEE International Conference on Robotics & Automation (ICRA)
Hong Kong Convention and Exhibition Center
May 31 - June 7, 2014. Hong Kong, China

Stationary Balance Control of a Bikebot

Yizhai Zhang, Pengcheng Wang, Jingang Yi, Dezhen Song, and Tao Liu

Abstract— **We present the development of the gyroscopic-balanced control of an autonomous bikebot. The bikebot is an actively controlled bicycle-based robotic platform with a gyro-balancer developed to study human dynamic postural balance motor skills through unstable physical human-robot interactions. We also present a dynamic model and analysis for stationary bikebot. A nonlinear balancing controller is designed to stabilize the underactuated stationary bikebot on an orbital trajectory around the unstable equilibrium point that is coupled with another orbit of the actuated gyro-balancer. We then demonstrate the analysis and control design with experimental validations. Finally, we present a set of human riding experiments to show how the bikebot can be used to perturb and excite human sensorimotor feedback loop for dynamic postural balance motor skills.**

I. Introduction

Robotic systems have been introduced and used in biomechanics, neuroscience, and human movement science to study human postural balance. Those mechanical systems include one or two degree-of-freedom (DOF) moving plates (e.g., [1]), or multi-DOF robotic platforms (e.g., [2]) for testing dynamic posturography. However, few robotic devices are designed to aim at studying or training the human's whole-body postural capability through unstable physical human-robot interactions. We consider using the newly developed bikebot as a new means to examine a sensorimotor theory for modeling and shaping postural balancing and other functional whole-body motor activities. Although studying physical interactions between the rider and the passive bicycle is reported in recent years [3]–[6], the bikebot provides active perturbation to break rider's sensorimotor feedback loop through actively controlled steering, velocity, and balancing. In addition, compared to other motor skills such as quiet stance [7], riding the bikebot requires the coordinated control of multi-limb and body movements following the sensorimotor cues. Therefore, the bikebot offers a new platform for studying human postural balance motor skills through unstable physical human-robot interactions.

Bikebot is an actively controlled bicycle-based robot. Our bikebot concept was inspired by the recent clinical studies in [8], [9] that report promising results of treating postural disorder and Parkinson's disease patients through bicycle riding. The bicycle-based rehabilitation device in [8] is a stationary platform and does not have the capability for dynamically sensing and perturbing human motor control skills. Our previous works [4]–[6] introduce a non-intrusive instrumented bicycle system and this type of instrumented bicycles however cannot actively perturb human motion and break the human neural control feedback loop. The bikebot instead extends the capability of the instrumented bicycle by modified steering, driving and balancing mechanisms to augment the rider's dynamic postural balance capability.

In this paper, we focus on the dynamic modeling, balance control for stationary bikebot system and present the feasibility to study rider's balance control by using bikebot. The dynamic model of the riderless gyro-balancer bicycle is first developed. We analyze the bikebot stationary dynamic model and present a pair of coupled oscillating orbits for the bikebot roll motion and a flywheel's pivoting motion. The balancing control design is then to regulate the bikebot motions through the gyro-balancer to follow these orbital trajectories. An energy shaping method is used to design the orbital following controller. We present experiments to demonstrate the balancing analysis and control design. Finally, human riding experiments are presented to show the feasibility of using bikebot to perturb and excite human sensorimotor postural balance feedback mechanisms.

Besides the new bikebot design and demonstrating the feasibility to perturb and excite human postural balance control, additional contributions of this work are twofold. First, the presented stationary bikebot dynamic model captures a class of underactuated robotic systems in which the coupled effects between the actuated component (gyro-balancer) and the underactuated component (bikebot roll motion) are through force/torque and energy exchange. Following the modeling analysis, we propose a coupled orbital following control design to balance the bikebot. This design complements the orbital stabilization approach in [10], [11] where virtual displacement constraints, rather than force/torque constraints, are introduced and used. Second, comparing with other related work in which autonomous motorcycles or bicycles are designed at a moving velocity [12]–[19], we have successfully demonstrated a more challenging task to balance the stationary bikebot on orbit at zero velocity. Moreover, we analytically give an estimation of the domain of attraction under the control design.

The remainder of the paper is organized as follows. We discuss the bikebot dynamic model in Section II. The balancing control and analysis are presented in Section III. Experiments are presented in Section IV and we finally

This work was supported in part by the US National Science Foundation under awards CMMI-0954966 and CMMI-1334389.

Y. Zhang is with the Department of Control and Information, School of Automation, Northwestern Polytechnical University, Xi'an, Shaanxi 710072 China and the Key Laboratory of Information Fusion Technology (LIFT), Ministry of Education, China (e-mail: yzzhang@nwpu.edu.cn).

P. Wang and J. Yi are with the Department of Mechanical and Aerospace Engineering, Rutgers University, Piscataway, NJ 08854 USA (e-mail: pengcheng.wang@rutgers.edu, jgyi@rutgers.edu).

D. Song is with the Department of Computer Science and Engineering, Texas A&M University, College Station, TX 77845 USA (e-mail: dzsong@cse.tamu.edu).

T. Liu is with the Department of Mechanical Engineering, Zhejiang University, Hangzhou 310027 China (e-mail: liutao@zju.edu.cn).

978-1-4799-3684-7/14/$31.00 ©2014 IEEE

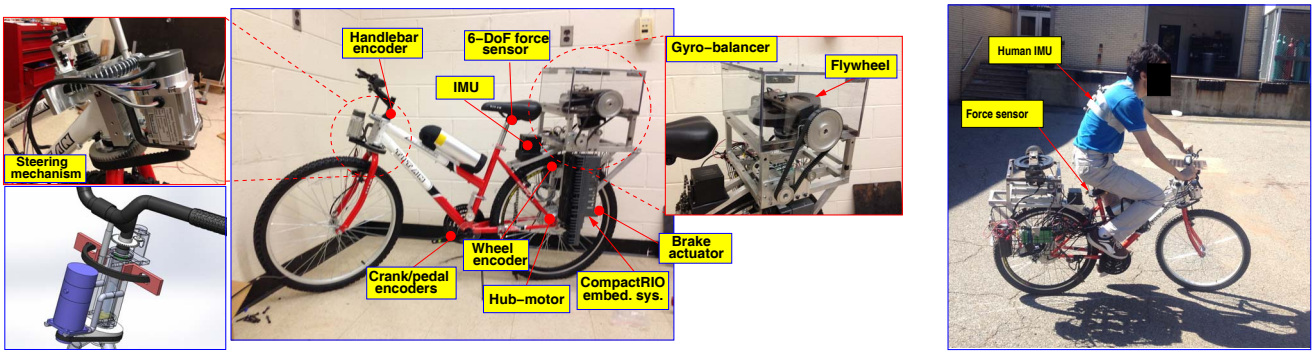

(a) (b)

Fig. 1. (a) The Rutgers bikebot for studying physical rider-robot interactions. The left sub-figure shows the modified steering mechanism that disengages the rider steering with the actual motorized steering fork. The right-figure shows the single gyro-balancer design. (b) Human riding experiment.

conclude the paper in Section V.

II. Bikebot Dynamic Model

Fig. 1(a) shows the bikebot developed at Rutgers University. The mechanical structure of the bikebot is built on a mountain bicycle with significant modifications. Both the traction/braking and the steering functions are augmented to allow a human rider, an onboard computer, or both to balance the unstable platform. A hub motor and a DC motor are used for rear-wheel driving and front steering mechanism control, respectively. The steering mechanism is modified such that the steering handlebar and the steering fork are mechanical separated and independently controlled; see the left sub-figure in Fig. 1(a). The rider turns the handlebar and the onboard controller can turn the lower-steering mechanism at a commanded steering angle. Same design is applied to pedaling for control the bikebot moving velocity. To perturb the rider's balancing torque, a single gimbal active controlled gyro-balancer is mounted on the back rack of the bikebot as shown in the right sub-figure in Fig. 1(a).

The bikebot is a three-part platform: a rear frame with the gyro-balancer structure and rear wheel, the front wheel and steering mechanism and the gyro-balance flywheel. Fig. 2 shows a schematic of the bikebot kinematics. We assume that the mass center W of the gyro-balancer is located at the rotating axis and therefore, its translational velocity is along the rear frame. We denote C_1 and C_2 as the front and rear wheel contact points with the ground, respectively. As shown in Fig. 2, frame $\mathcal{B}(x, y, z)$ is setup on the rear frame with its origin at C_2. Without pitch motion, yaw angle ψ and roll angle φ_b are used to capture bicycle motion and the unit vector set of $\mathcal{B}$ is denoted as $(\boldsymbol{i}, \boldsymbol{j}, \boldsymbol{k})$.

From [20], the vertical position change Δh_G of the mass center G due to steering angle ϕ is captured as

$$\Delta h_G = l_G \Delta_s \tan\varphi_b \tan\phi, \tag{1}$$

where $\Delta_s = \frac{l_t \cos\xi}{l}\left[l_t \cos\xi - \frac{12 R_t \xi}{\pi^2}\left(1 - \frac{\sqrt{3}}{2}\right)\right]$, R_t is the radius of the front wheel, ξ is the caster angle, l and l_t are the wheelbase and trail distance, respectively. The velocity of C_2 and the angular velocity of the rear frame in $\mathcal{B}$ are respectively given as $\boldsymbol{v}_{C_2} = v_x \boldsymbol{i}$ and $\boldsymbol{\omega}_b = \dot{\varphi}_b \boldsymbol{i} + \dot{\psi}\, \mathrm{s}_{\varphi_b} \boldsymbol{j} + \dot{\psi}\, \mathrm{c}_{\varphi_b} \boldsymbol{k}$, where v_x is moving forward velocity and we use notations $\mathrm{c}_{\varphi_b} := \cos\varphi_b$ and $\mathrm{s}_{\varphi_b} := \sin\varphi_b$ for φ_b and other

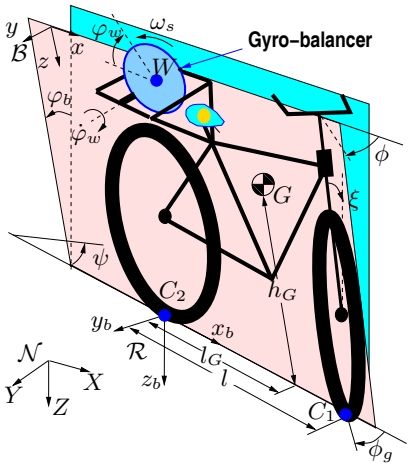

Fig. 2. Schematic of the gyro-balanced bikebot systems.

angles. The position of G in $\mathcal{B}$ is $\boldsymbol{\rho}_G = l_G \boldsymbol{i} - h_G \boldsymbol{k}$, where l_G and h_G are the horizontal and vertical distances from G to C_2, respectively. We thus obtain the velocity of G as $\boldsymbol{v}_G = (v_x - h_G \dot{\psi}\, \mathrm{s}_{\varphi_b})\boldsymbol{i} + (h_G \dot{\varphi}_b + l_G \dot{\psi}\, \mathrm{c}_{\varphi_b})\boldsymbol{j} - l_G \dot{\psi}\, \mathrm{s}_{\varphi_b} \boldsymbol{k}$. The flywheel's precession angular velocity is $\boldsymbol{\Omega}_w = \dot{\varphi}_b \boldsymbol{i} + (\dot{\psi}\, \mathrm{s}_{\varphi_b} + \dot{\varphi}_w)\boldsymbol{j} + \dot{\psi}\, \mathrm{c}_{\varphi_b} \boldsymbol{k}$, where φ_w is the flywheel pivoting angle. The gyroscopic torque generated by the gyro-balancer along the x-axis direction is obtained

$$\begin{aligned}\tau_{wx} = {} & (I_{wz} - I_{wx})(\dot{\psi}^2\, \mathrm{c}_{\varphi_b}\, \mathrm{s}_{\varphi_b} + \dot{\psi}\dot{\varphi}_w\, \mathrm{c}_{\varphi_b}) + \\ & I_{wz}\omega_s\, \mathrm{c}_{\varphi_w}(\dot{\psi}\, \mathrm{s}_{\varphi_b} + \dot{\varphi}_w)\end{aligned} \tag{2}$$

where the flywheel inertia matrix is $\boldsymbol{I}_w = \mathrm{diag}\{I_{wx}, I_{wy}, I_{wz}\}$ with the assumption that the principle axes are along its body frame.

With the nonholonomic constraint at C_2 and the kinematic geometry [20], we obtain that $v_x = \frac{l}{\sigma}\dot{\psi}$ and $\sigma = \tan\phi_g$ and $\tan\phi_g\, \mathrm{c}_\varphi = \tan\phi\, \mathrm{c}_\xi$. Using the constrained Lagrange approach [3], [14], we obtain the motion equations of the bikebot. Considering a stationary bikebot, $v_x = 0$ and $\dot{\psi} = 0$, the bikebot motion equations are reduced to

$$\begin{aligned}&(m_b h_G^2 + I_x + I_{wxz}\, \mathrm{s}^2_{\varphi_w})\ddot{\varphi}_b + I_{wxz}\, \mathrm{s}_{2\varphi_w}\, \dot{\varphi}_w \dot{\varphi}_b - m_b g h_G\, \mathrm{s}_{\varphi_b} \\ &+ I_{wz}\, \mathrm{c}_{\varphi_w}\, \dot{\varphi}_w \omega_s = m_b g l_G \Delta_s \sec^2\varphi_b \tan\phi, \end{aligned} \tag{3}$$

$$I_{wy}\ddot{\varphi}_w + I_{wxz}\dot{\varphi}_b^2\, \mathrm{c}_{\varphi_w}\, \mathrm{s}_{\varphi_w} - I_{wz}\dot{\varphi}_b \omega_s\, \mathrm{c}_{\varphi_w} = \tau_m, \tag{4}$$

where $I_{wxz} = I_{wz} - I_{wx}$.

III. Stationary Balancing Control and Analysis

We define state variable $\boldsymbol{x} = [x_1 \quad x_2 \quad x_3]^T = [\varphi_b \quad \dot{\varphi}_b \quad \sin\varphi_w]^T$. For presentation convenience, we also define $\boldsymbol{x}_b = [x_1 \ x_2]^T$. Since the pivoting motor is controlled by the lower-level controller for a given velocity, we consider a velocity input for pivoting angle x_3. Thus, we re-write (3) along with the pivoting angular velocity control as

$$\dot{x}_1 = x_2 \tag{5a}$$
$$\dot{x}_2 = f(\boldsymbol{x}) + g_1(\boldsymbol{x})u_1 + g_2(\boldsymbol{x})u_2 \tag{5b}$$
$$\dot{x}_3 = u_1, \tag{5c}$$

where $u_1 = \mathrm{c}_{\varphi_w}\dot{\varphi}_w$ is the controlled pivoting velocity, $u_2 = \tan\phi$ is the controlled steering input,

$$f(\boldsymbol{x}) = \frac{m_b g h_G \,\mathrm{s}_{x_1}}{I_s(\boldsymbol{x})},\ g_1(\boldsymbol{x}) = -\frac{2I_{wxz}x_2x_3 + I_{wz}\omega_s}{I_s(\boldsymbol{x})},$$
$$g_2(\boldsymbol{x}) = \frac{m_b g l_G \Delta_s \sec^2 x_1}{I_s(\boldsymbol{x})}, \tag{6}$$

and $I_s(\boldsymbol{x}) = m_b h_G^2 + I_x + I_{wxz}x_3^2$. Due to the physical constraints, the pivoting angle and angular rate are within certain ranges, namely,

$$|x_3| = |\,\mathrm{s}_{\varphi_w}\,| \le \mathrm{s}_{\varphi_w^{\max}} < 1,\ |u_1| = |\,\mathrm{c}_{\varphi_w}\dot{\varphi}_w| \le \omega_w^{\max}, \tag{7}$$

where $\varphi_w^{\max}$ and $\omega_w^{\max}$ are the maximum flywheel pivoting angle and angular velocity, respectively.

Without steering control (i.e., $u_2 = 0$), the equilibrium of the dynamics (5) is $x_{1e} = x_{2e} = 0$ under $u_{1e} = \dot{\varphi}_{we} = 0$. It is interesting to notice that the flywheel pivoting angle can be any values within $\varphi_w^{\max}$ while the bikebot is balanced.

We consider how to compute the gyro-balancer flywheel's pivoting angle $x_3(t)$ for a given profile for bikebot roll angle $x_1(t)$. Indeed, (3) can be re-written as

$$\frac{d}{dt}\Big[(m_b h_G^2 + I_x)x_2 + I_{wxz}\dot{\varphi}_b x_3^2 + I_{wz}\omega_s x_3\Big] = -\frac{\partial}{\partial\varphi_b}\Big(m_b g h_G\,\mathrm{c}_{x_1}\Big) \tag{8}$$

and thus, the bikebot satisfies the Hamiltonian dynamics with angular momentum along the x-axis direction

$$p_x(t) = (m_b h_G^2 + I_x)x_2(t) + I_{wxz}x_2(t)x_3^2(t) + I_{wz}\omega_s x_3(t). \tag{9}$$

By integrating (8), it is then straightforward to obtain

$$p_x(t) - p_x(0) = \int_0^t m_b g h_G\,\mathrm{s}_{x_1(\tau)}\,d\tau. \tag{10}$$

We have the following property with the proof given in appendix.

Property 1: For a given periodic profile $x_1(t)$ with period T, the profile for the pivoting angle is also periodic with period T.

With the results in Property 1, we design an orbital stabilization control to synchronize the periodic motion between the flywheel pivoting (x_3) and the bikebot roll motion (x_1).

The balancing controller is designed by using the gyro-balancer. To further simplify the controller design, from (6) and the fact that the flywheel spinning speed $\omega_s \gg |x_2|$, it is noted that $I_{wz}\omega_s \gg |2I_{wxz}x_2x_3|$. Moreover, $m_b h_G^2 \gg I_x \gg I_{wxz}$ and therefore, (5b) is approximated as

$$\dot{x}_2 - \frac{g}{h_G}\,\mathrm{s}_{x_1} + \frac{I_{wz}\omega_s}{m_b h_G^2}u_1 = 0. \tag{11}$$

Clearly, for simplified dynamics (11), state variable $\boldsymbol{x} \in \mathcal{D} := \mathbb{S}\times\mathbb{R}\times(-1,1)$.

We consider regulating the bikebot roll motion on an orbital trajectory in $\mathcal{D}$. An oscillation orbital trajectory $\mathcal{O}_b$ is given by the following pendulum dynamics.

$$\mathcal{O}_b:\ \dot{x}_2 + \frac{b}{h_G}\,\mathrm{s}_{x_1} = 0, \tag{12}$$

where design parameter $b > 0$ is a gravitationally equivalent constant. Plugging (12) into dynamics (11) to eliminate term s_{x_1}, we obtain

$$\dot{x}_3 = -\frac{(b+g)m_b h_G^2}{I_{wz}b\omega_s}\dot{x}_2 = -L\dot{x}_2, \tag{13}$$

where constant $L = \frac{(g+b)m_b h_G^2}{I_{wz}b\omega_s}$. Therefore, by integrating (13), the corresponding orbital trajectory $\mathcal{O}_w$ for x_3 is obtained as

$$\mathcal{O}_w:\ x_3 = -Lx_2. \tag{14}$$

Remark 1: The form of (14) is seemingly similar to those of virtual holonomic constraints in orbital stabilization of underactuated mechanical systems in [10], [11]. However, the relationships (14) are not the same as the virtual constraints in [10], [11] because (14) is obtained through the system dynamics (11) rather than by design. Moreover, (14) represents the torque balance relationship between the controlled flywheel pivoting and the underactuated bikebot roll motion, while the virtual holonomic constraints in [10], [11] capture the displacement relationships among the coordinates.

Once the bikebot roll motion follows orbit $\mathcal{O}_b$, the total energy $E(\boldsymbol{x}_b)$ is defined as:

$$E(\boldsymbol{x}_b) = \frac{1}{2}m_b h_G^2 x_2^2 + m_b h_G b\,(1 - \mathrm{c}_{x_1}).$$

When target orbit $\mathcal{O}_b$ reaches the maximum angle x_1^d with $x_2 = 0$, the total energy is $E_d = m_b h_G b(1 - \mathrm{c}_{x_1^d})$. We define the energy difference $\Delta E = E(\boldsymbol{x}_b) - E_d$ and consider the Lyapunov candidate function $V_1(\boldsymbol{x})$ as

$$V_1(\boldsymbol{x}) = \frac{1}{2}\Delta E^2 + \frac{1}{2}k_1\,(x_3 + Lx_2)^2,$$

where $k_1 > 0$ is a constant. Obviously, $V_1(\boldsymbol{x}) \ge 0$ and

$$\dot{V}_1(\boldsymbol{x}) = \Delta E(m_b h_G^2 x_2\dot{x}_2 + m_b h_G b\,\mathrm{s}_{x_1}x_2) + k_1(x_3 + Lx_2)(\dot{x}_3 + L\dot{x}_2).$$

Using (5) and (11) and letting

$$u_1 = \frac{Lb}{h_G}\,(\mathrm{s}_{x_1} + v_1) = u_{1s} + \frac{Lb}{h_G}v_1, \tag{15}$$

where $u_{1s} = \frac{Lb}{h_G}\,\mathrm{s}_{x_1}$ and v_1 is an auxiliary control input, $\dot{V}_1(\boldsymbol{x})$ is then reduced to $\dot{V}_1(\boldsymbol{x}) = -m_b h_G(g + b)\,[\Delta E x_2 + \alpha k_1\,(x_3 + Lx_2)]\,v_1$, where $\alpha = \frac{g}{bI_{wz}\omega_s} > 0$ is a constant.

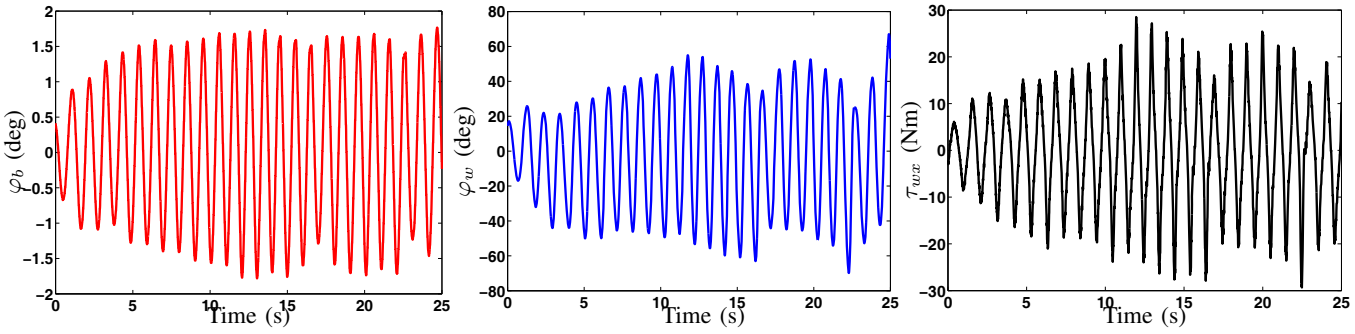

Fig. 3. Bikebot self-balancing at zero velocity using the gyro-balancer control. (a) Bikebot roll angle φ_b. (b) Gyro-balancer flywheel pivoting angle φ_w. (c) The controlled turning torque τ_{wx}.

The control input v_1 is further designed as

$$v_1 = k_2 \left[\Delta E x_2 + \alpha k_1 \left(x_3 + L x_2\right)\right] \tag{16}$$

with a positive constant parameter $k_2 > 0$ and then we obtain

$$\dot{V}_1(\boldsymbol{x}) = -m_b h_G (g+b) k_2 \left[\Delta E x_2 + \alpha k_1 \left(x_3 + L x_2\right)\right]^2 \leq 0.$$

By LaSalle theory [21], the system states asymptotically converge to the invariant set $\mathcal{S}(\boldsymbol{x})$

$$\mathcal{S}(\boldsymbol{x}) = \left\{\boldsymbol{x} \in \mathcal{D} \,|\Delta E x_2 + \alpha k_1 \left(x_3 + L x_2\right) = 0\right\}. \tag{17}$$

In $\mathcal{S}(\boldsymbol{x})$, $v_1 = 0$, $u_1 = u_{1s}$ and the trajectories of the closed-loop dynamics are on orbits $\mathcal{O}_b$ and $\mathcal{O}_w$. It is straightforward to obtain that origin $\boldsymbol{x}_e = \mathbf{0} \in \mathcal{S}(\boldsymbol{x})$.

If the states are not at origin in $\mathcal{S}(\boldsymbol{x})$, i.e., $\boldsymbol{x} \in \mathcal{S}(\boldsymbol{x}) \setminus \{\mathbf{0}\}$, ΔE is a constant with the periodical varying x_2 and from (13), we obtain $x_3 + L x_2 = C$ (constant). Given the invariant set property in (17), this implies that in $\mathcal{S}(\boldsymbol{x}) \setminus \{\mathbf{0}\}$, $E = E_d$ (i.e., $\Delta E = 0$) and $x_3 + L x_2 = 0$. Thus, a subset of the invariant orbit $\mathcal{O}_w$ given by

$$\mathcal{O}_w^*(\boldsymbol{x}) = \left\{\boldsymbol{x} \in \mathcal{D} \,|\Delta E = 0,\, x_3 + L x_2 = 0\right\}$$

also lies in $\mathcal{S}(\boldsymbol{x})$, namely, $\mathcal{O}_w^* = \mathcal{S}(\boldsymbol{x}) \setminus \{\mathbf{0}\}$. By LaSalle principle, under the control (15), the state variables converge to the target orbits $\mathcal{O}_b$ and $\mathcal{O}_w^*$ asymptotically for an initial state $\boldsymbol{x}(0)$ in the domain of attraction $\mathcal{D}_1 \subset \mathcal{D}$. We give an estimate of the domain of attraction $\mathcal{D}_1$ under the gyro-balancer control (15). From the previous analysis, under control (15), $\boldsymbol{x} \in \mathcal{S}(\boldsymbol{x})$, $\dot{V}_1(\boldsymbol{x}) = 0$, and $\boldsymbol{x} = \mathbf{0}$, $V_1(\mathbf{0}) = \frac{1}{2} E_d^2$; $\boldsymbol{x} \in \mathcal{O}_w^*(\boldsymbol{x})$, $\dot{V}_1(\boldsymbol{x}) = 0$. Therefore, a conservative estimate of $\mathcal{D}_1$ is

$$\mathcal{D}_1(\boldsymbol{x}) = \left\{\boldsymbol{x} \in \mathcal{D} \,|\, V_1(\boldsymbol{x}) \leq \frac{1}{2} E_d^2\right\}. \tag{18}$$

IV. Experiments

The physical parameter values of the bikebot are obtained experimentally and listed in Table I. A force/torque sensor (from JR3 Inc.) is installed along the seat supporting rod to measure the 3-axis hip-seat forces and torques; see Fig. 1(a). An optical encoder is used to measure the bicycle speed. One IMU unit (model 800 from Motion Sense Inc.) is mounted to the bicycle frame to obtain bicycle attitude estimation. For human riding experiment, a second IMU is attached at the back of the rider to measure the upper-body pose [6]; see Fig. 1(b). The embedded system (NI cRIO 9082 real-time system) samples and stores all sensor measurements and also controls the motors at the frequency of 100 Hz.

TABLE I
Bikebot Physical Parameters

m_b (kg)	I_{bx} (kgm^2)	I_{wx} (kgm^2)	I_{wz} (kgm^2)	h_G (m)
51	2.5	0.028	0.036	0.64
l_G (m)	l (m)	l_t (m)	ξ (deg)	R_t (m)
0.27	1.1	0.06	20	0.33

We demonstrate the gyro-balancer-based control of the stationary bikebot in experiments. The gyro-balancer-based balancing controller (15) was implemented at constant $\omega_s = 1080$ rpm with well-tuned parameter $b = 1$, $k_1 = 1.3$ and $k_2 = 1$ and the bikebot was successfully balanced. Fig. 3 shows the experimental results. The bikebot roll angle is shown in Fig. 3(a), the gyro-balancer flywheel pivoting angle is shown in Fig. 3(b) and the generated gyroscopic balancing torque is shown in Fig. 3(c). Clearly, the trajectories of the bikebot roll angle and the pivoting angle converge to the orbits and are finally synchronized in a periodic motion. It is also clear that under the gyro-balancer control constraint (7), the bikebot can be balanced within a small range (i.e., 2-3 degs.) around the vertical position.

The synchronized motion between the bikebot roll and flywheel pivoting motions can be further observed from the phase portraits shown in Fig. 4. Fig. 4(a) shows the phase portrait of the bikebot roll motion, Fig. 4(b) of the flywheel pivoting motion and Fig. 4(c) is the domain of attraction estimation (18) projected on the roll motion plane. The results shown in these plots confirm the design of the orbital stabilization design and also demonstrate that the controlled bikebot motion is within the DOA estimate.

To demonstrate the feasibility of the use of the bikebot to perturb the human motor control, we also conduct a set of human riding experiments. A young male subject with experienced bicycle riding skills rode the bikebot in outdoor environment (Fig. 1(b)) with his regular riding style. Both a straight-line riding (for a distance of 50 m) and a circular riding (about a radius of 3 m) were conducted in experiments. The riding speeds were among 2-3 m/s range. After the

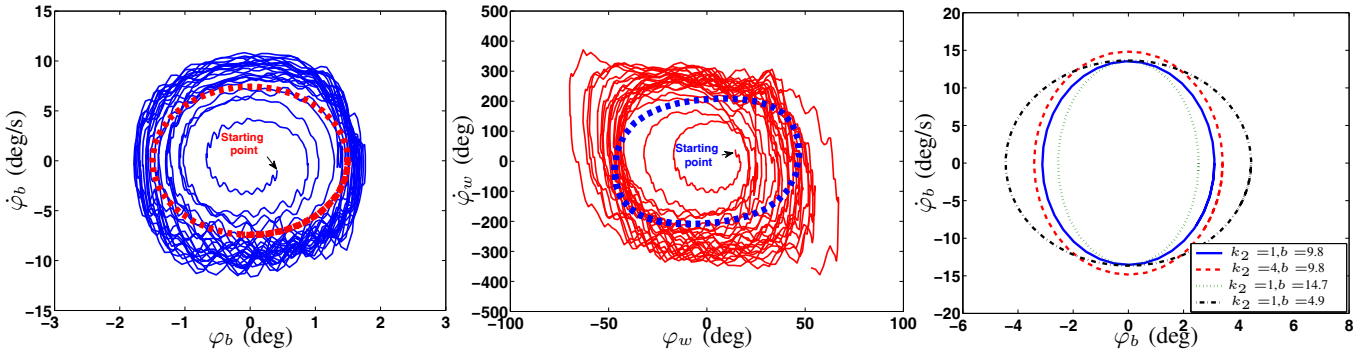

(a) (b) (c)

Fig. 4. Phase portraits of the stationary bikebot self-balancing control. (a) Bikebot roll motion $\dot{\varphi}_b$ vs. φ_b. The thick dashed line indicates the orbit $\mathcal{O}_b$. (b) Gyro-balancer flywheel motion $\dot{\varphi}_w$ vs. φ_w. The thick dashed line indicates the orbit $\mathcal{O}_w$. (c) The estimated $\mathcal{D}_1$ projected on plane φ_b-$\dot{\varphi}_b$.

subject got used to ride the bikebot comfortably, we turned on the gyro-balancer to perturb the riding and measured the rider's responses to the generated torque disturbances.

We first perturbed the riding by a single torque disturbance suddenly applied without notifying the rider. Fig. 5 shows the steering angle responses and the perturbed torques for both the straight-line and circular bikebot riding experiments. It is clearly shown in these plots that under a perturbation, the rider uses the steering as a motor control strategy to keep balancing the unstable platform. The responses also confirm the "counter-steering" strategy (turning the steering toward the same direction as falling trend), a bicycle-riding motor skill that is obtained through training.

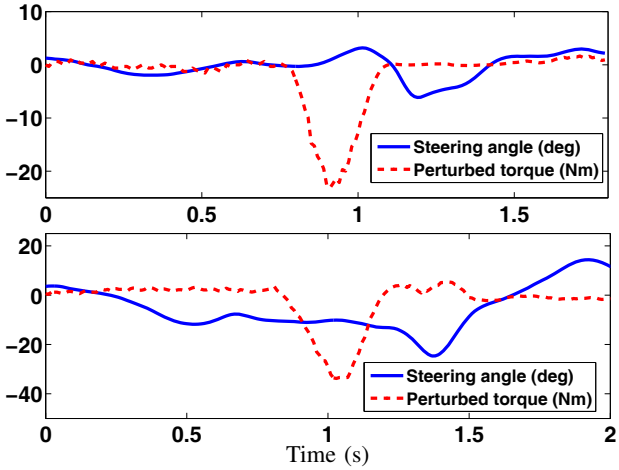

Fig. 5. Steering angle and a single perturbed torque disturbance. Top: along a straight-line trajectory. Bottom: along a circular trajectory.

To further demonstrate that riders use steering, rather than other motor strategies such as upper body motions, as an effective strategy in the straight-line and circular riding, we conduct riding experiments under randomly generated torques. We compare the riding responses in these perturbed experiments with profiles obtained from normally riding experiments without any disturbances. Fig. 6 shows the comparison results of the rider-bikebot interactions under a normal and a perturbed experiment. Fig. 6(a)-6(c) shows the rider's steering angle responses, bikebot roll angle, and the rider applied torque in the roll angle direction for straight-line riding and Fig. 6(d)-6(f) shows the profiles of the same variables for circular riding experiments. The rider responded to the random perturbation by actively turning the handlebar and using steering to balance the platform in experiments. This is clearly observed by the comparison with normal riding behavior shown in Fig. 6(a) and 6(d). On the other hand, neither of the comparisons of the bikebot roll angle profiles shown in Fig. 6(b) and 6(e) nor rider applied torques shown in Fig. 6(b) and 6(e) does clearly demonstrate significant difference. These results and observations confirm that the bikebot platform can be used to study dynamic postural human motor skills.

V. Conclusion

We reported the development of the bikebot for studying human dynamic postural balance motor control. The bikebot was modified from a bicycle platform to argument the rider's capability with actuated steering, driving and balancing capabilities. This paper presented a dynamic model of the bikebot with a gyro-balancer actuator. A self-balancing control was designed to stabilize the riderless, underactuated stationary bikebot on motion orbits. The stability and the stable regions were also obtained through analysis. We demonstrated the controller design and analysis through experiments. Riding experiments were also presented to demonstrate the feasibility to use the bikebot platform to study and tune human dynamic postural control.

References

[1] A. D. Goodworth and R. J. Peterka, "Influence of bilateral vestibular loss on spinal stabilization in humans," *J. Neurophysiol.*, vol. 103, pp. 1978–1987, 2010.

[2] F. Patané and P. Cappa, "A 3-DOF parallel robot with spherical motion for the rehabilitation and evaluation of balance performance," *IEEE Trans. Neural Syst. Rehab. Eng.*, vol. 19, no. 2, pp. 157–166, 2011.

[3] Y. Zhang and J. Yi, "Dynamic modeling and balance control of human/bicycle systems," in *Proc. IEEE/ASME Int. Conf. Adv. Intell. Mechatronics*, Montreal, Canada, 2010, pp. 1385–1390.

[4] J. Yi, D. Soudbakhsh, Y. Zhang, and Y. Zhang, "Why some Parkinson's disease patients cannot stand or walk but can ride a bicycle – A control system-based analysis," in *Proc. ASME Dyn. Syst. Control Conf.*, Ft. Lauderdale, FL, 2012, Paper # DSCC2012-8735.

[5] K. Chen, Y. Zhang, and J. Yi, "Modeling rider/bicycle interactions with learned dynamics on constrained embedding manifolds," in *Proc. IEEE/ASME Int. Conf. Adv. Intell. Mechatronics*, Wollongong, Australia, 2013, pp. 442–447.

[6] Y. Zhang, K. Chen, and J. Yi, "Rider trunk and bicycle pose estimation with fusion of force/inertial sensors," *IEEE Trans. Biomed. Eng.*, vol. 60, no. 9, pp. 2541–2551, 2013.

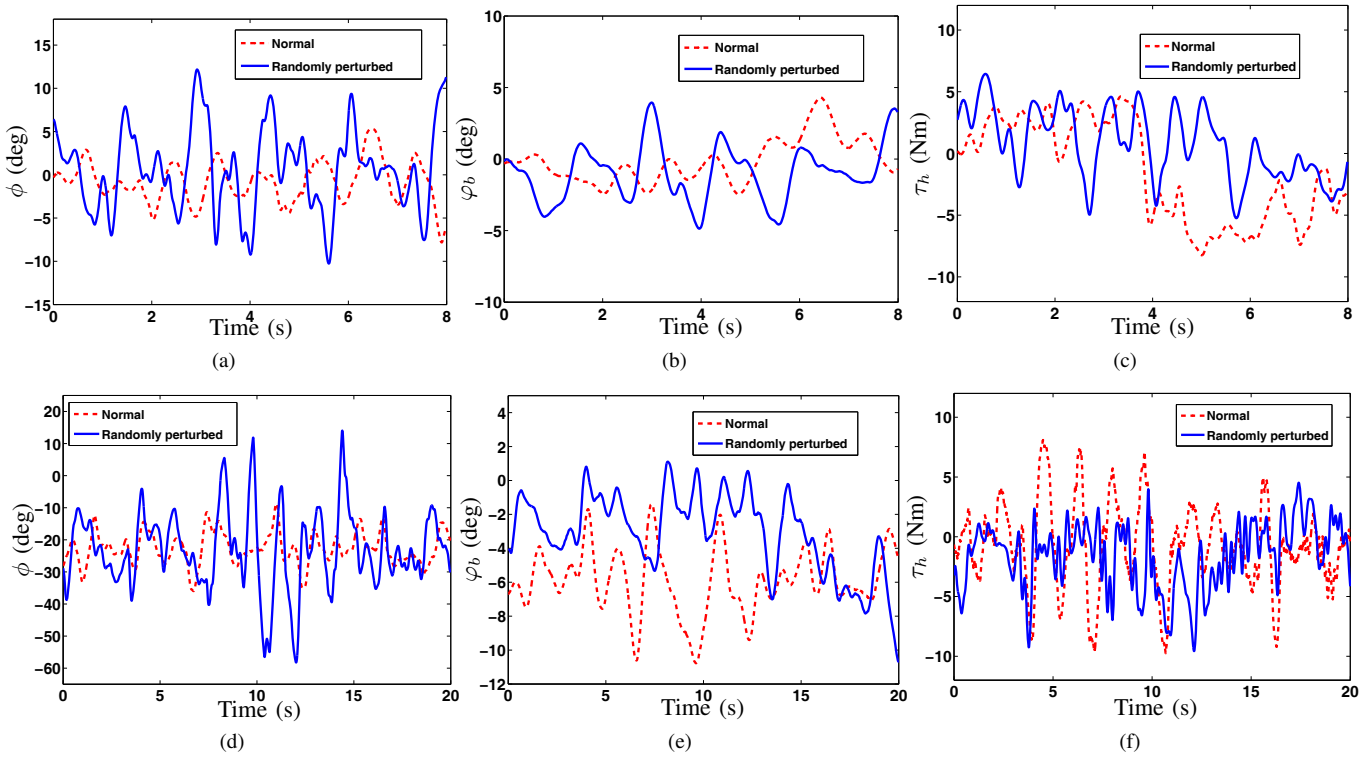

Fig. 6. Rider-bikebot responses under typical riding and randomly perturbation by the gyro-balancer for the straight-line (top row) and circular (bottom row) trajectories. (a) Steering angle ϕ for straight-line. (b) Bikebot roll angle φ_b for straight-line. (c) Rider applied torque τ_h on the seat for straight-line. (d) Steering angle ϕ for straight-line. (e) Bikebot roll angle φ_b for straight-line. (f) Rider applied torque τ_h on the seat for straight-line.

[7] H. van der Kooij, R. Jocob, B. Koopman, and H. Grootenboer, "A multisensory integration model of human stance control," *Biol. Cybern.*, vol. 80, pp. 299–308, 1999.

[8] C.-G. Song, J.-Y. Kim, and N.-G. Kim, "A new postural balance control system for rehabilitation training based on virtual cycling," *IEEE Trans. Inform. Technol. Biomed.*, vol. 8, no. 2, pp. 200–207, 2004.

[9] M. B. Aerts, W. F. Abdo, and B. R. Bloem, "The "bicycle sign" for atypical parkinsonism," *Lancet*, vol. 377, pp. 125–126, 2011.

[10] A. S. Shiriaev, J. W. Perram, and C. Canudas-de-Wit, "Constructive tool for orbital stabilization of underactuated nonlinear systems: Virtual constraints approach," *IEEE Trans. Automat. Contr.*, vol. 50, no. 8, pp. 1164–1176, 2005.

[11] A. S. Shiriaev, L. B. Freidovich, A. Robertsson, R. Johansson, and A. Sandberg, "Virtual-holonomic-constraints-based design of stable oscillations of Furuta pendulum: Theory and experiments," *IEEE Trans. Robotics*, vol. 23, no. 4, pp. 827–832, 2007.

[12] A. Beznos, A. Formal'sky, E. Gurfinkel, D. Jicharev, A. Lensky, K. Savitsky, and L. Tchesalin, "Control of autonomous motion of two-wheel bicycle with gyroscopic stabilisation," in *Proc. IEEE Int. Conf. Robot. Autom.*, Leuven, Belgium, 1998, pp. 2670–2675.

[13] S. Lee and W. Ham, "Self-stabilzing strategy in tracking control of unmanned electric bicycle with mass balance," in *Proc. IEEE/RSJ Int. Conf. Intell. Robot. Syst.*, Lausanne, Switzerland, 2002, pp. 2200–2205.

[14] J. Yi, D. Song, A. Levandowski, and S. Jayasuriya, "Trajectory tracking and balance stabilization control of autonomous motorcycles," in *Proc. IEEE Int. Conf. Robot. Autom.*, Orlando, FL, 2006, pp. 2583–2589.

[15] B. T. Thanh and M. Parnichkun, "Balancing control of bicyrobo by particle swarm optimization-based structure-specified mixed H_2/H_∞ control," *Int. J. Adv. Robotic Syst.*, vol. 5, no. 4, pp. 395 – 402, 2008.

[16] V. Cerone, D. Andreo, M. Larsson, and D. Regruto, "Stabilization of a riderless bicycle: A linear-parameter-varying approach," *IEEE Control Syst. Mag.*, vol. 30, no. 5, pp. 23–32, 2010.

[17] Y. Tanaka and T. Murakami, "A study on straight-line tracking and posture control in electric bicycle," *IEEE Trans. Ind. Electron.*, vol. 56, no. 1, pp. 159–168, 2009.

[18] L. Keo and M. Yamakita, "Control of an autonomous electric bicycle with both steering and balancer controls," *Adv. Robot.*, vol. 25, no. 1-2, pp. 1–22, 2011.

[19] J. D. G. Kooijman, J. Merjaard, J. M. Papadopoulos, A. Ruina, and A. Schwab, "A bicycle can be self-stable without gyroscopic or caster effects," *Science*, vol. 332, pp. 339–342, 2011.

[20] Y. Zhang, J. Li, J. Yi, and D. Song, "Balance control and analysis of stationary riderless motorcycles," in *Proc. IEEE Int. Conf. Robot. Autom.*, Shanghai, China, 2011, pp. 3018–3023.

[21] H. K. Khalil, *Nonlinear Systems*, 3rd ed. Upper Saddle River, NJ: Prentice Hall, 2002.

APPENDIX

For a periodic profile $x_1(t+T) = x_1(t)$ for any t, $x_2(t) = \dot{x}_1(t)$ is also periodic with period T, i.e., $x_2(t+T) = x_2(t)$. From (10), we obtain

$$p_x(t+T) - p_x(0) = \int_0^{t+T} m_b g h_G \, \mathrm{s}_{x_1(\tau)} \, d\tau.$$

Taking the difference of the above equation with (10), we obtain

$$p_x(t+T) - p_x(t) = \int_0^{T} m_b g h_G \, \mathrm{s}_{x_1(\tau)} \, d\tau. \qquad (19)$$

Using the fact that both $x_1(t)$ and $x_2(t)$ are periodic functions with period T and $\int_0^T \mathrm{s}_{x_1(\tau)} \, d\tau = 0$, using (9), (19) reduces to

$$[x_3(t+T) - x_3(t)]\,[I_{wz}\omega_s + I_{wxz}(x_3(t+T) + x_3(t))] = 0.$$

Thus, $x_3(t+T) = x_3(t)$ and the flywheel's pivoting angle is periodic with period T. This completes the proof.